Measurement of $e^+e^- \to \gamma\chi_{cJ}$ via initial state radiation at Belle

Y. L. Han,[18] X. L. Wang,[64] C. Z. Yuan,[18] C. P. Shen,[2] P. Wang,[18] A. Abdesselam,[55] I. Adachi,[14,10] H. Aihara,[61] S. Al Said,[55,28] D. M. Asner,[50] T. Aushev,[39,22] V. Babu,[56] I. Badhrees,[55,27] V. Bansal,[50] V. Bhardwaj,[54] J. Biswal,[23] A. Bozek,[45] M. Bračko,[35,23] A. Chen,[43] B. G. Cheon,[12] R. Chistov,[22] K. Cho,[29] V. Chobanova,[36] S. -K. Choi,[11] D. Cinabro,[65] J. Dalseno,[36,57] M. Danilov,[22,38] Z. Doležal,[4] A. Drutskoy,[22,38] D. Dutta,[56] S. Eidelman,[3,48] H. Farhat,[65] J. E. Fast,[50] T. Ferber,[7] B. G. Fulsom,[50] V. Gaur,[56] N. Gabyshev,[3,48] A. Garmash,[3,48] D. Getzkow,[8] R. Gillard,[65] R. Glattauer,[19] Y. M. Goh,[12] P. Goldenzweig,[25] B. Golob,[33,23] J. Haba,[14,10] K. Hayasaka,[41] H. Hayashii,[42] X. H. He,[51] T. Horiguchi,[59] W. -S. Hou,[44] T. Iijima,[41,40] A. Ishikawa,[59] I. Jaegle,[13] D. Joffe,[26] K. K. Joo,[5] H. Kichimi,[14] D. Y. Kim,[53] J. B. Kim,[30] J. H. Kim,[29] K. T. Kim,[30] S. H. Kim,[12] Y. J. Kim,[29] K. Kinoshita,[6] B. R. Ko,[30] P. Kodyš,[4] P. Križan,[33,23] P. Krokovny,[3,48] P. Lewis,[13] L. Li Gioi,[36] J. Libby,[16] D. Liventsev,[64,14] P. Lukin,[3,48] M. Masuda,[60] D. Matvienko,[3,48] K. Miyabayashi,[42] H. Miyata,[46] R. Mizuk,[22,38] A. Moll,[36,57] H. K. Moon,[30] R. Mussa,[21] E. Nakano,[49] M. Nakao,[14,10] M. Nayak,[16] N. K. Nisar,[56] S. Nishida,[14,10] S. Ogawa,[58] S. Okuno,[24] W. Ostrowicz,[45] P. Pakhlov,[22,38] G. Pakhlova,[39,22] B. Pal,[6] H. Park,[31] T. K. Pedlar,[34] R. Pestotnik,[23] M. Petrič,[23] L. E. Piilonen,[64] C. Pulvermacher,[25] E. Ribežl,[23] M. Ritter,[36] A. Rostomyan,[7] H. Sahoo,[13] Y. Sakai,[14,10] S. Sandilya,[56] L. Santelj,[14] T. Sanuki,[59] O. Schneider,[32] G. Schnell,[1,15] C. Schwanda,[19] K. Senyo,[66] M. E. Sevior,[37] M. Shapkin,[20] V. Shebalin,[3,48] T. -A. Shibata,[62] J. -G. Shiu,[44] B. Shwartz,[3,48] F. Simon,[36,57] Y. -S. Sohn,[67] A. Sokolov,[20] E. Solovieva,[22] S. Stanič,[47] M. Steder,[7] M. Sumihama,[9] U. Tamponi,[21,63] Y. Teramoto,[49] M. Uchida,[62] S. Uehara,[14,10] T. Uglov,[22,39] Y. Unno,[12] S. Uno,[14,10] Y. Usov,[3,48] C. Van Hulse,[1] P. Vanhoefer,[36] G. Varner,[13] A. Vossen,[17] M. N. Wagner,[8] Y. Watanabe,[24] K. M. Williams,[64] S. Yashchenko,[7] Y. Yook,[67] C. C. Zhang,[18] Z. P. Zhang,[52] V. Zhilich,[3,48] V. Zhulanov,[3,48] and A. Zupanc[23]

(Belle Collaboration)

[1]*University of the Basque Country UPV/EHU, 48080 Bilbao*
[2]*Beihang University, Beijing 100191*
[3]*Budker Institute of Nuclear Physics SB RAS, Novosibirsk 630090*
[4]*Faculty of Mathematics and Physics, Charles University, 121 16 Prague*
[5]*Chonnam National University, Kwangju 660-701*
[6]*University of Cincinnati, Cincinnati, Ohio 45221*
[7]*Deutsches Elektronen–Synchrotron, 22607 Hamburg*
[8]*Justus-Liebig-Universität Gießen, 35392 Gießen*
[9]*Gifu University, Gifu 501-1193*
[10]*SOKENDAI (The Graduate University for Advanced Studies), Hayama 240-0193*
[11]*Gyeongsang National University, Chinju 660-701*
[12]*Hanyang University, Seoul 133-791*
[13]*University of Hawaii, Honolulu, Hawaii 96822*
[14]*High Energy Accelerator Research Organization (KEK), Tsukuba 305-0801*
[15]*IKERBASQUE, Basque Foundation for Science, 48013 Bilbao*
[16]*Indian Institute of Technology Madras, Chennai 600036*
[17]*Indiana University, Bloomington, Indiana 47408*
[18]*Institute of High Energy Physics, Chinese Academy of Sciences, Beijing 100049*
[19]*Institute of High Energy Physics, Vienna 1050*
[20]*Institute for High Energy Physics, Protvino 142281*
[21]*INFN - Sezione di Torino, 10125 Torino*
[22]*Institute for Theoretical and Experimental Physics, Moscow 117218*
[23]*J. Stefan Institute, 1000 Ljubljana*
[24]*Kanagawa University, Yokohama 221-8686*
[25]*Institut für Experimentelle Kernphysik, Karlsruher Institut für Technologie, 76131 Karlsruhe*
[26]*Kennesaw State University, Kennesaw GA 30144*
[27]*King Abdulaziz City for Science and Technology, Riyadh 11442*
[28]*Department of Physics, Faculty of Science, King Abdulaziz University, Jeddah 21589*
[29]*Korea Institute of Science and Technology Information, Daejeon 305-806*
[30]*Korea University, Seoul 136-713*
[31]*Kyungpook National University, Daegu 702-701*
[32]*École Polytechnique Fédérale de Lausanne (EPFL), Lausanne 1015*
[33]*Faculty of Mathematics and Physics, University of Ljubljana, 1000 Ljubljana*
[34]*Luther College, Decorah, Iowa 52101*
[35]*University of Maribor, 2000 Maribor*
[36]*Max-Planck-Institut für Physik, 80805 München*

 © 2015 American Physical Society

[37]*School of Physics, University of Melbourne, Victoria 3010*
[38]*Moscow Physical Engineering Institute, Moscow 115409*
[39]*Moscow Institute of Physics and Technology, Moscow Region 141700*
[40]*Graduate School of Science, Nagoya University, Nagoya 464-8602*
[41]*Kobayashi-Maskawa Institute, Nagoya University, Nagoya 464-8602*
[42]*Nara Women's University, Nara 630-8506*
[43]*National Central University, Chung-li 32054*
[44]*Department of Physics, National Taiwan University, Taipei 10617*
[45]*H. Niewodniczanski Institute of Nuclear Physics, Krakow 31-342*
[46]*Niigata University, Niigata 950-2181*
[47]*University of Nova Gorica, 5000 Nova Gorica*
[48]*Novosibirsk State University, Novosibirsk 630090*
[49]*Osaka City University, Osaka 558-8585*
[50]*Pacific Northwest National Laboratory, Richland, Washington 99352*
[51]*Peking University, Beijing 100871*
[52]*University of Science and Technology of China, Hefei 230026*
[53]*Soongsil University, Seoul 156-743*
[54]*University of South Carolina, Columbia, South Carolina 29208*
[55]*Department of Physics, Faculty of Science, University of Tabuk, Tabuk 71451*
[56]*Tata Institute of Fundamental Research, Mumbai 400005*
[57]*Excellence Cluster Universe, Technische Universität München, 85748 Garching*
[58]*Toho University, Funabashi 274-8510*
[59]*Tohoku University, Sendai 980-8578*
[60]*Earthquake Research Institute, University of Tokyo, Tokyo 113-0032*
[61]*Department of Physics, University of Tokyo, Tokyo 113-0033*
[62]*Tokyo Institute of Technology, Tokyo 152-8550*
[63]*University of Torino, 10124 Torino*
[64]*CNP, Virginia Polytechnic Institute and State University, Blacksburg, Virginia 24061*
[65]*Wayne State University, Detroit, Michigan 48202*
[66]*Yamagata University, Yamagata 990-8560*
[67]*Yonsei University, Seoul 120-749*

(Received 17 June 2015; published 20 July 2015)

The process $e^+e^- \to \gamma\chi_{cJ}$ ($J = 1, 2$) is studied via initial state radiation using 980 fb^{-1} of data at and around the $\Upsilon(nS)$ ($n = 1, 2, 3, 4, 5$) resonances collected with the Belle detector at the KEKB asymmetric-energy e^+e^- collider. No significant signal is observed except from $\psi(2S)$ decays. Upper limits on the cross sections between $\sqrt{s} = 3.80$ and 5.56 GeV are determined at the 90% credibility level, which range from a few pb to a few tens of pb. We also set upper limits on the decay rate of the vector charmonium [$\psi(4040)$, $\psi(4160)$, and $\psi(4415)$] and charmoniumlike [$Y(4260)$, $Y(4360)$, and $Y(4660)$] states to $\gamma\chi_{cJ}$.

DOI: 10.1103/PhysRevD.92.012011 PACS numbers: 14.40.Pq, 13.25.Gv, 13.66.Bc

In e^+e^- annihilation, the energy region above the $D\bar{D}$ threshold is rich with vector charmonium and charmoniumlike states. Three charmoniumlike states with $J^{PC} = 1^{--}$ were discovered at B factories via initial state radiation (ISR) in the last decade: the $Y(4260)$ in $e^+e^- \to \pi^+\pi^- J/\psi$ [1,2] and the $Y(4360)$ and $Y(4660)$ in $e^+e^- \to \pi^+\pi^-\psi(2S)$ [3,4]. Together with the conventional charmonium states $\psi(4040)$, $\psi(4160)$, and $\psi(4415)$, there are six vector states; the potential models predict only five in this mass region [5]. Some of these states show unusual properties that are inconsistent with charmonium [6]. It is unlikely that all of these states are charmonia; some, perhaps, have exotic nature: a multiquark state, molecule, hybrid, or some other configuration. To improve our understanding of these states and the underlying QCD, it is important to investigate them using much larger data samples and new decay channels.

For example, one can study radiative transitions between these states and lower charmonium states like the χ_{cJ}. The CLEO Collaboration used data taken during a scan of center-of-mass (CM) energies $\sqrt{s} = 3.97$–4.26 GeV to report upper limits on the cross sections of $e^+e^- \to \gamma\chi_{c1}$ and $e^+e^- \to \gamma\chi_{c2}$ in three energy regions: the $\psi(4040)$ ($\sqrt{s} = 3.97$–4.06 GeV), the $\psi(4160)$ (4.12–4.20 GeV), and $\sqrt{s} = 4.26$ GeV [7]. The limited statistics prevented them from measuring the line shape of $e^+e^- \to \gamma\chi_{cJ}$. The BESIII experiment reports the upper limits on the cross sections of the reactions $e^+e^- \to \gamma\chi_{c1}$ and $e^+e^- \to \gamma\chi_{c2}$ at four energy points: $\sqrt{s} = 4.009$, 4.230, 4.260, and 4.360 GeV [8]. With the full Belle data sample, we are able to study this process via ISR.

In this paper, we report a study of the $e^+e^- \to \gamma\chi_{cJ}$ process using ISR events detected with the Belle

detector [9] at the KEKB asymmetric-energy e^+e^- collider [10]. Here, χ_{cJ} is reconstructed in the $\gamma J/\psi$ final state and J/ψ is reconstructed in the $\mu^+\mu^-$ final state alone (the background level is very high in the e^+e^- final state due to Bhabha events). The same final state $\gamma\gamma J/\psi$ has been previously analyzed at Belle and $\psi(4040)$ and $\psi(4160)$ were observed as $\eta J/\psi$ resonances [11]. We study the full Belle data set corresponding to an integrated luminosity of 980 fb^{-1}. About 70% of the data was collected at the $\Upsilon(4S)$ resonance, and the remainder was taken at the other $\Upsilon(nS)$ ($n = 1$, 2, 3, or 5) states or at CM energies a few tens of MeV lower than the $\Upsilon(4S)$ or the $\Upsilon(nS)$ peaks.

The event generator EVTGEN [12] with the VECTORISR model is used to simulate the signal process $e^+e^- \to \gamma_{\rm ISR}V \to \gamma_{\rm ISR}\gamma\chi_{cJ} \to \gamma_{\rm ISR}\gamma\gamma J/\psi$. The mass and width of V can be varied so that we can obtain the signal efficiency as a function of the vector meson mass. This model considers the leading-order (LO) quantum electrodynamics (QED) correction only and thus higher-order corrections should be estimated and properly taken into account. The dedicated ISR generator PHOKHARA [13] has the next-to-leading-order (NLO) QED correction but does not contain the mode of interest. However, the process $e^+e^- \to \gamma_{\rm ISR}V \to \gamma_{\rm ISR}\eta J/\psi$ can be generated with PHOKHARA and this allows us to estimate the NLO correction effect in the mode under study by comparing the results from the two generators in the analysis of the $\eta J/\psi$ mode. All generated events are passed through the GEANT3 [14] based detector simulation and then the standard reconstruction.

For a candidate event, we require two good charged tracks with zero net charge. The impact parameters of these tracks perpendicular to and along the beam direction with respect to the interaction point are required to be less than 0.5 and 5.0 cm, respectively. The transverse momentum of the leptons is required to be greater than 0.1 GeV/c. For each charged track, information from different detector subsystems is combined to form a likelihood $\mathcal{L}_i$ for each particle species (i) [15]. For muons from $J/\psi \to \mu^+\mu^-$, one of the tracks is required to have the muon identification (μID) likelihood ratio $\mathcal{R}_\mu = \frac{\mathcal{L}_\mu}{\mathcal{L}_\mu+\mathcal{L}_\pi} > 0.95$; in addition, if one of the muon candidates has no μID information [16], the polar angle of each muon candidate in the $\gamma\chi_{cJ}$ CM system is required to satisfy $|\cos\theta_\mu| < 0.75$. The lepton ID efficiency is about 87% for $J/\psi \to \mu^+\mu^-$.

A photon candidate is an electromagnetic calorimeter cluster with energy $E(\gamma) > 50$ MeV that does not match any charged tracks. The photon is labeled as the ISR photon when its energy in the e^+e^- CM frame exceeds 3 GeV (corresponding to $M[\gamma\chi_{cJ}] < 7$ GeV/c^2, the maximum non-ISR photon energy being about 3 GeV) and this photon is excluded when reconstructing $\gamma\chi_{cJ}$ candidates. We also require at least two additional photons, each with energy in the laboratory frame greater than 0.25 GeV. Among these, we select the two with the highest energy in the laboratory system and denote these as γ_h and γ_l (with $E_{\gamma_h} > E_{\gamma_l}$). The detection of the ISR photon is not required; instead, we require -1 (GeV/c^2)$^2 < M^2_{\rm rec} <$ 2 (GeV/c^2)^2, where $M^2_{\rm rec}$ is the square of the mass recoiling against the $\gamma\chi_{cJ}$ system. The distribution of $M^2_{\rm rec}$ is shown in Fig. 1.

Figure 2 shows the $\mu^+\mu^-$ invariant mass [$M(\mu^+\mu^-)$] distribution for events that survive the selection criteria and the $\gamma_l\gamma_h J/\psi$ invariant mass [$M(\gamma_l\gamma_h J/\psi) = M(\gamma_l\gamma_h\mu^+\mu^-) - M(\mu^+\mu^-) + m_{J/\psi}$] less than 5.56 GeV/$c^2$, where $m_{J/\psi}$ is the nominal mass of the J/ψ [17]. A $\mu^+\mu^-$ pair is considered as a J/ψ candidate if $M(\mu^+\mu^-)$ is within ± 45 MeV/c^2 (the mass resolution being 15 MeV/c^2) of the J/ψ nominal mass [17]. The J/ψ mass sidebands are defined as $M(\mu^+\mu^-) \in [3.172, 3.262]$ GeV/c^2 or $[2.932, 3.022]$ GeV/c^2, which are twice as wide as the signal region.

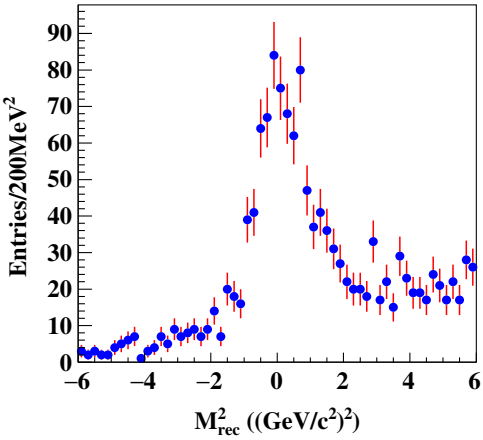


FIG. 1 (color online). Missing mass squared distribution with $M(\gamma_l\gamma_h J/\psi) < 5.56$ GeV/c^2.

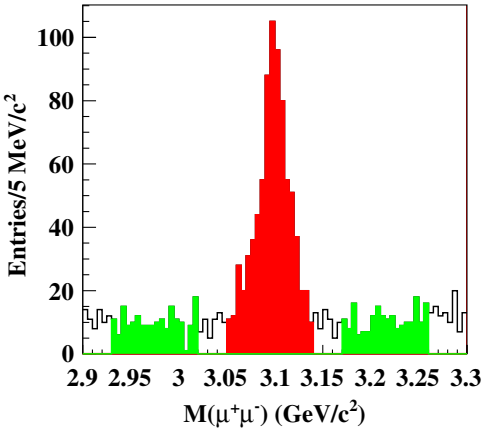


FIG. 2 (color online). Invariant mass distribution of $\mu^+\mu^-$. The shaded area in the middle is the J/ψ signal region, and the shaded regions on either side are the J/ψ mass sidebands.

To reject the background from $e^+e^- \to \gamma_{\rm ISR}\eta(\pi^0)J/\psi$ events with η or π^0 decaying into two photons, we require that the invariant mass of the two photons, $M(\gamma\gamma)$, be outside the η mass region of $[0.50, 0.58]$ GeV/c^2, the π^0 mass region, and the low-invariant-mass region $M(\gamma\gamma) < 0.20$ GeV/c^2. Figure 3 shows the invariant mass distribution of $M(\gamma J/\psi)$ [with two entries per event for $M(\gamma_h J/\psi)$ and $M(\gamma_l J/\psi)$] for events with $M(\gamma_l\gamma_h J/\psi) < 5.56$ GeV/c^2. Here, $M(\gamma_{l(h)}J/\psi) = M(\gamma_{l(h)}\mu^+\mu^-) - M(\mu^+\mu^-) + m_{J/\psi}$. We observe χ_{c1} and χ_{c2} signals but no evidence of χ_{c0}. We divide the χ_{cJ} mass region into $[3.48, 3.535]$ GeV/c^2 for χ_{c1} and $[3.535, 3.58]$ GeV/c^2 for χ_{c2}.

Figure 4 shows the $M(\gamma_l\gamma_h J/\psi)$ distribution after applying all the selection criteria above. We see a clear $\psi(2S)$ signal but no significant signal in the higher mass region.

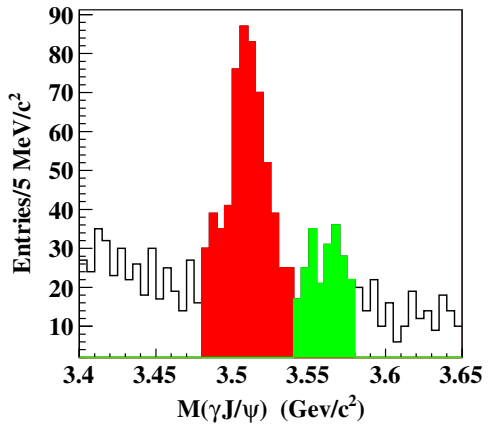


FIG. 3 (color online). Invariant mass distribution of $\gamma J/\psi$ for candidate events with $M(\gamma_l\gamma_h J/\psi) < 5.56$ GeV/c^2. The shaded histograms show the $\chi_{c1}([3.48, 3.535]$ GeV/$c^2)$ and $\chi_{c2}([3.535, 3.58]$ GeV/$c^2)$ regions.

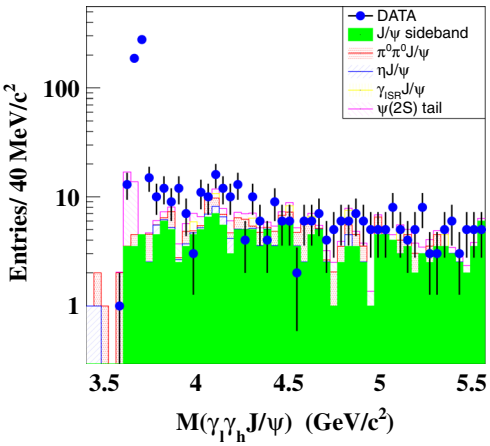


FIG. 4 (color online). Invariant mass distribution of $\gamma_l\gamma_h J/\psi$. The background from the tail of the $\psi(2S)$ is plotted only for $M(\gamma_l\gamma_h J/\psi) > 3.75$ GeV/c^2 and $M(\gamma_l\gamma_h J/\psi) < 3.65$ GeV/c^2. The dots with error bars are data while the shaded histograms represent different sources of background modes.

The clear χ_{cJ} and $\psi(2S)$ signals allow us to measure the product branching fractions $\mathcal{B}[\psi(2S) \to \gamma\chi_{cJ}] \times \mathcal{B}[\chi_{cJ} \to \gamma J/\psi]$ $(J = 1, 2)$. By contrast, in the region $M(\gamma\gamma J/\psi) \in [3.80, 5.56]$ GeV/c^2, we set an upper limit on the production cross section of $e^+e^- \to \gamma\chi_{cJ}$.

The potential backgrounds are also shown in Fig. 4. Besides the non-J/ψ background, which also appear in the J/ψ mass sidebands, there are three additional backgrounds: $e^+e^- \to \gamma_{\rm ISR}J/\psi$, $\gamma_{\rm ISR}\pi^0\pi^0 J/\psi$, and $\gamma_{\rm ISR}\eta J/\psi$. Of course, $e^+e^- \to \gamma_{\rm ISR}\psi(2S)$ with $\psi(2S) \to \gamma\chi_{cJ}$ will be a background in the analysis of the $\gamma_l\gamma_h J/\psi$ high-mass region. The ISR J/ψ and $\psi(2S)$ samples are generated according to the theoretical calculation of the production cross sections [18] with the world-average resonant parameters as input [17]. For the other modes, we use the cross sections of $e^+e^- \to \eta J/\psi$ [11] and $e^+e^- \to \pi^+\pi^- J/\psi$ [19] and assume that $\sigma(e^+e^- \to \pi^0\pi^0 J/\psi) = \frac{1}{2}\sigma(e^+e^- \to \pi^+\pi^- J/\psi)$. All these samples are generated using the PHOKHARA generator [13] and are normalized to the integrated luminosity of the full data sample. The background contribution practically saturates the mass spectrum above the $\psi(2S)$ peak.

To measure the $\psi(2S) \to \gamma\chi_{cJ}$ branching fractions, we define the $\psi(2S)$ signal region as 3.65 GeV/c^2 < $M(\gamma_l\gamma_h J/\psi) < 3.72$ GeV/c^2. The distribution of the energy of the less energetic photon in the $\gamma_l\gamma_h J/\psi$ CM system is shown in Fig. 5. Clear signals due to χ_{c1} and χ_{c2} are observed with very low background and we fit this photon energy distribution to extract the corresponding yields. The χ_{cJ} signal shapes are obtained from Monte Carlo simulated signal samples convolved with a corresponding smearing Gaussian function to compensate

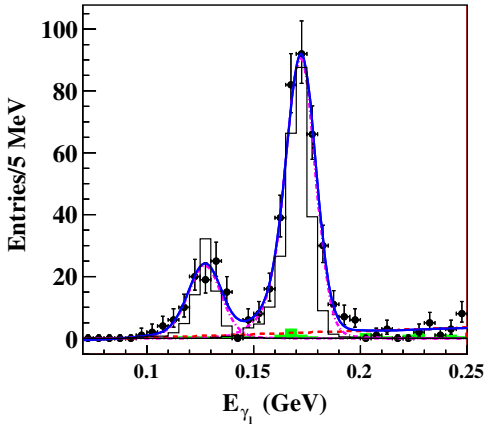


FIG. 5 (color online). Energy distributions of the low energy photon in the $\gamma_l\gamma_h J/\psi$ CM system for events in the $\psi(2S)$ mass region. Dots with error bars are data and histograms are MC samples. The blue solid line is the best fit, the red dashed line is the shape of the total background determined from the fit, and the purple dot-dashed line is the MC signal shape convolved with a Gaussian function. The shaded histogram shows the total background as determined from J/ψ sidebands and simulations.

for the resolution difference between data and Monte Carlo simulation; the background is parametrized as a first-order Chebyshev polynomial. The resulting fit function is shown in Fig. 5 and the fit yields 340 ± 20 χ_{c1} and 97 ± 12 χ_{c2} signal events.

From the world-average $\psi(2S)$ resonant parameters [17], we calculate $\sigma[e^+e^- \to \gamma_{\rm ISR}\psi(2S)] = (14.25 \pm 0.26)$ pb [18] and thus expect 13.9×10^6 ISR produced $\psi(2S)$ events in the full Belle data sample of 980 fb^{-1}. With the efficiencies of 1.4% and 0.7% for the χ_{c1} and χ_{c2} modes, respectively, from the MC simulation, we obtain $\mathcal{B}[\psi(2S) \to \gamma\chi_{c1}] \times \mathcal{B}(\chi_{c1} \to \gamma J/\psi) = (2.92 \pm 0.19)\%$ and $\mathcal{B}[\psi(2S) \to \gamma\chi_{c2}] \times \mathcal{B}(\chi_{c2} \to \gamma J/\psi) = (1.65 \pm 0.21)\%$. Here, the errors are statistical only. These results are consistent with the PDG values [17].

The $M(\gamma_l\gamma_h J/\psi)$ distributions above the $\psi(2S)$ signal region for $\gamma\chi_{c1}$ and $\gamma\chi_{c2}$ candidate events as well as their sum are shown in Fig. 6, together with the background estimation from the J/ψ mass sidebands and the MC simulated background modes with a genuine J/ψ. No significant signal is observed in either the $\gamma\chi_{c1}$ or $\gamma\chi_{c2}$ mode. As the background estimation is limited to the known channels, it only serves as a lower limit of the true background. In calculating the upper limits of the $\gamma\chi_{cJ}$ production cross section, we consider the estimated-background events from the observed signal candidates. This results in a conservative estimate of the upper limit of the signal and hence a conservative estimate for the cross section.

There is cross contamination between the χ_{c1} and χ_{c2} signals due to the mass resolution, as can be seen from Fig. 3, and this is taken into account as follows. The yields of observed χ_{c1} and χ_{c2} events (denoted as $n_{\rm obs}^{\chi_{c1}}$ and $n_{\rm obs}^{\chi_{c2}}$, respectively) are expressed as

$$\begin{pmatrix} n_{\rm obs}^{\chi_{c1}} \\ n_{\rm obs}^{\chi_{c2}} \end{pmatrix} = \begin{pmatrix} \epsilon_{11} & \epsilon_{21} \\ \epsilon_{12} & \epsilon_{22} \end{pmatrix} \begin{pmatrix} N^{\chi_{c1}} \times \mathcal{B}(\chi_{c1} \to \gamma J/\psi) \times \mathcal{B}(J/\psi \to \mu^+\mu^-) \\ N^{\chi_{c2}} \times \mathcal{B}(\chi_{c2} \to \gamma J/\psi) \times \mathcal{B}(J/\psi \to \mu^+\mu^-) \end{pmatrix} + \begin{pmatrix} n_{\rm bkg}^{\chi_{c1}} \\ n_{\rm bkg}^{\chi_{c2}} \end{pmatrix}. \quad (1)$$

In these equations, ϵ_{ij} $(i, j = 1, 2)$ is the efficiency of produced χ_{ci} to be reconstructed in the χ_{cj} signal region; $N^{\chi_{c1}}$ and $N^{\chi_{c2}}$ represent the total numbers of χ_{c1} and χ_{c2} events produced in data, respectively; $\mathcal{B}$ is the world-average branching fraction for the given process [17]; and $n_{\rm bkg}^{\chi_{c1}}$ and $n_{\rm bkg}^{\chi_{c2}}$ represent the numbers of non-χ_{cJ} background events for χ_{c1} and χ_{c2}, respectively, which are the sum of the normalized J/ψ mass sideband background

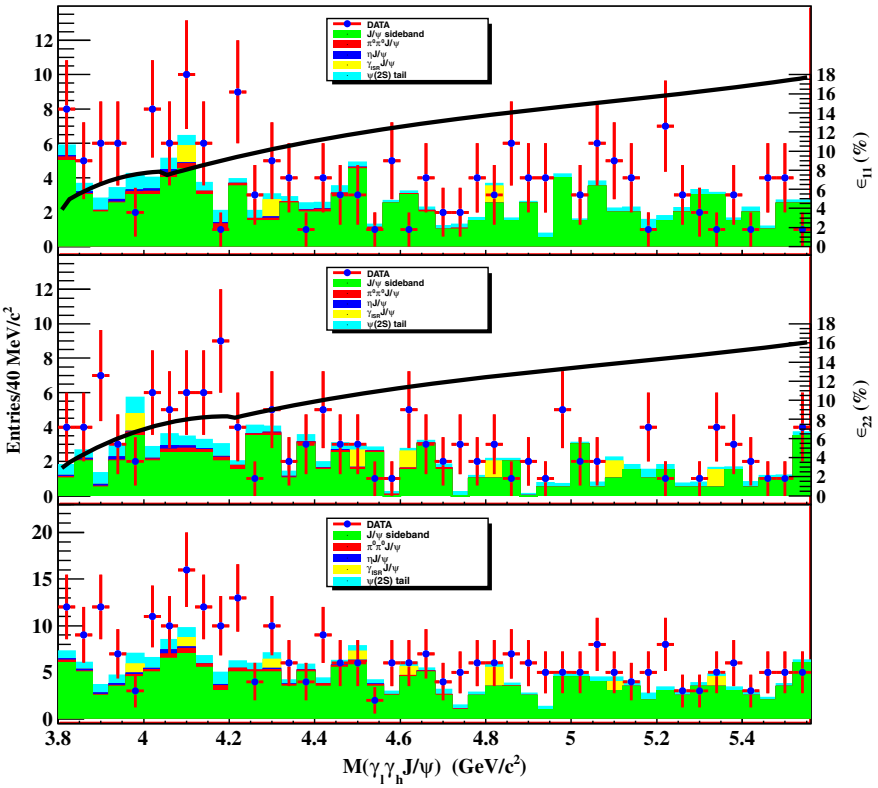


FIG. 6 (color online). Invariant mass distributions of $\gamma\chi_{cJ}$ candidates. Shown from top to bottom are $\gamma\chi_{c1}$, $\gamma\chi_{c2}$, and their sum. Dots with error bars are data, the shaded histograms are the simulated backgrounds and J/ψ sidebands, and the solid lines are the efficiency curves.

and the MC simulated $\gamma_{\rm ISR}J/\psi$, $\gamma_{\rm ISR}\eta J/\psi$, $\gamma_{\rm ISR}\pi^0\pi^0 J/\psi$, and $\gamma_{\rm ISR}\psi(2S)$ background, as shown in Fig. 6. The efficiency curves ϵ_{11} and ϵ_{22}, also shown in Fig. 6, are not monotonic between $3.9\ {\rm GeV}/c^2 < m(\gamma\chi_{cJ}) < 4.2\ {\rm GeV}/c^2$. This is due to the fact that the energies of the two photons are almost the same in this mass region.

We use the maximum likelihood method to determine upper limits on the numbers of produced $\gamma\chi_{cJ}$ events, $N^{\chi_{c1}}$ and $N^{\chi_{c2}}$, and thus on the upper limits of the production cross sections of $e^+e^- \to \gamma\chi_{cJ}$. The likelihood is constructed as follows. For each possible pair of the $N^{\chi_{c1}}$ and $N^{\chi_{c2}}$ values, the numbers of the expected signal events, $\nu^{\chi_{c1}}$ and $\nu^{\chi_{c2}}$, are

$$\begin{pmatrix}\nu^{\chi_{c1}}\\ \nu^{\chi_{c2}}\end{pmatrix} = \begin{pmatrix}\epsilon_{11} & \epsilon_{21}\\ \epsilon_{12} & \epsilon_{22}\end{pmatrix}\begin{pmatrix}N^{\chi_{c1}}\times\mathcal{B}(\chi_{c1}\to\gamma J/\psi)\times\mathcal{B}(J/\psi\to\mu^+\mu^-)\\ N^{\chi_{c2}}\times\mathcal{B}(\chi_{c2}\to\gamma J/\psi)\times\mathcal{B}(J/\psi\to\mu^+\mu^-)\end{pmatrix}. \quad (2)$$

Taking into account the background contribution, the numbers of expected events in the signal regions, denoted as $\mu^{\chi_{c1}}$ and $\mu^{\chi_{c2}}$ for χ_{c1} and χ_{c2}, respectively, are

$$\begin{pmatrix}\mu^{\chi_{c1}}\\ \mu^{\chi_{c2}}\end{pmatrix} = \begin{pmatrix}\nu^{\chi_{c1}}\\ \nu^{\chi_{c2}}\end{pmatrix} + \begin{pmatrix}n^{\chi_{c1}}_{\rm bkg}\\ n^{\chi_{c2}}_{\rm bkg}\end{pmatrix}, \quad (3)$$

and the probability of observing $\begin{pmatrix}n^{\chi_{c1}}_{\rm obs}\\ n^{\chi_{c2}}_{\rm obs}\end{pmatrix}$ events in data is

$$p(N^{\chi_{c1}}, N^{\chi_{c2}}) = \frac{(\mu^{\chi_{c1}})^{n^{\chi_{c1}}_{\rm obs}} e^{-\mu^{\chi_{c1}}}}{n^{\chi_{c1}}_{\rm obs}!}\frac{(\mu^{\chi_{c2}})^{n^{\chi_{c2}}_{\rm obs}} e^{-\mu^{\chi_{c2}}}}{n^{\chi_{c2}}_{\rm obs}!}. \quad (4)$$

The uncertainty in the background estimation is considered by sampling $n^{\chi_{cJ}}_{\rm bkg}$ in Eq. (3). By fitting the normalized background distribution, the mean value and the uncertainty of the background level are obtained. The background yield $n^{\chi_{cJ}}_{\rm bkg}$ is varied assuming it follows a Gaussian distribution with this mean value and the uncertainty as the standard deviation. The systematic error of the measurement, which corresponds to an uncertainty in the expected number of events, follows a Gaussian distribution with a mean value $\nu^{\chi_{cJ}}$ and a standard deviation $\nu^{\chi_{cJ}}\times\sigma_{\rm sys}$, where $\sigma_{\rm sys}$ is the total relative systematic error (13.4%), described below. This is also considered by varying $\mu^{\chi_{cJ}}$ in Eq. (4).

The summation of random-sampled $p(N^{\chi_{c1}}, N^{\chi_{c2}})$, considering the uncertainty in background estimation and the systematic errors, forms the final likelihood function

$$\begin{aligned}L(N^{\chi_{c1}}, N^{\chi_{c2}}) &= \frac{1}{N}\sum_{k,l,m,n} p(N^{\chi_{c1}}, N^{\chi_{c2}})\\ &= \frac{1}{N}\sum_{k,l,m,n}\frac{(\mu^{\chi_{c1}}_{k,l})^{n^{\chi_{c1}}_{\rm obs}} e^{-\mu^{\chi_{c1}}_{k,l}}}{n^{\chi_{c1}}_{\rm obs}!}\frac{(\mu^{\chi_{c2}}_{m,n})^{n^{\chi_{c2}}_{\rm obs}} e^{-\mu^{\chi_{c2}}_{m,n}}}{n^{\chi_{c2}}_{\rm obs}!}.\end{aligned} \quad (5)$$

Here, N is the number of samplings. $\mu^{\chi_{c1}}_{k,l} = \nu^{\chi_{c1}}_k + n^{\chi_{c1}}_{{\rm bkg},l}$ and $\mu^{\chi_{c2}}_{m,n} = \nu^{\chi_{c2}}_m + n^{\chi_{c2}}_{{\rm bkg},n}$, where $\nu^{\chi_{c1}}_k$, $n^{\chi_{c1}}_{{\rm bkg},l}$, $\nu^{\chi_{c2}}_m$, and $n^{\chi_{c2}}_{{\rm bkg},n}$ are the numbers of events obtained from the corresponding Gaussian distributions. The subscript k represents the kth sampling for the expected number of χ_{c1} signal events $\nu^{\chi_{c1}}$. The other subscripts l, m, and n have parallel meanings. By letting $N^{\chi_{c1}}$ and $N^{\chi_{c2}}$ run over all the possible values from 0 to infinity independently, we obtain the likelihood in the $(N^{\chi_{c1}}, N^{\chi_{c2}})$ plane. The likelihood $L(N^{\chi_{c1}})$ can be obtained from this two-dimensional likelihood function by integrating over the variable $N^{\chi_{c2}}$. From this, we obtain the upper limit on $N^{\chi_{c1}}$ at the 90% credibility level (C.L.)[1] and convert this into the upper limit on $\sigma(e^+e^-\to\gamma\chi_{c1})$. The upper limit on $\sigma(e^+e^-\to\gamma\chi_{c2})$ is determined in a similar manner. The final upper limits are shown in Fig. 7 and are around a few pb to a few tens of pb. We also show the CLEO and BESIII results in Fig. 7 for comparison. The measured upper limits are more stringent than the CLEO results at $\sqrt{s} = 3.97$–4.06 GeV and $\sqrt{s} = 4.26$ GeV. The large data samples collected by BESIII at $\sqrt{s} = 4.009$, 4.230, 4.260, and 4.360 GeV provide stronger upper limits at these energy points. The values of the upper limits measured here are listed in Table I.

We extract the transition rate of the vector charmonium and charmoniumlike states to $\gamma\chi_{cJ}$ by fitting the distributions in Fig. 6. We use a Breit-Wigner function for the signal and a first- or second-order polynomial function for the background. While doing the fit, the mass and total width are fixed to the world-average values [17] and $\Gamma_{ee}\times\mathcal{B}(R\to\gamma\chi_{cJ})$ is scanned from zero to a large number at which the probability is less than 1.0% of the largest value. Normalized probability density functions are derived from such a scan. These probability density functions then give the upper limits at 90% C.L. as listed in Table II. Taking $\Gamma_{ee}[\psi(4040)]$ and $\Gamma_{ee}[\psi(4415)]$ from the world-average values [17] and $\Gamma_{ee}[\psi(4160)]$ from the BES II measurement [20], we set the upper limits on the branching fractions for these three conventional charmonium states as listed in Table III. Taking $\Gamma_{ee}[Y(4260)]\times\mathcal{B}[Y(4260)\to\pi^+\pi^- J/\psi] = (6.4\pm0.8\pm0.6)$ eV or $(20.5\pm1.4\pm2.0)$ eV [19] [there

[1]In common high energy physics usage, this Bayesian interval has been reported as "confidence interval" which is a frequentist-statistics term.

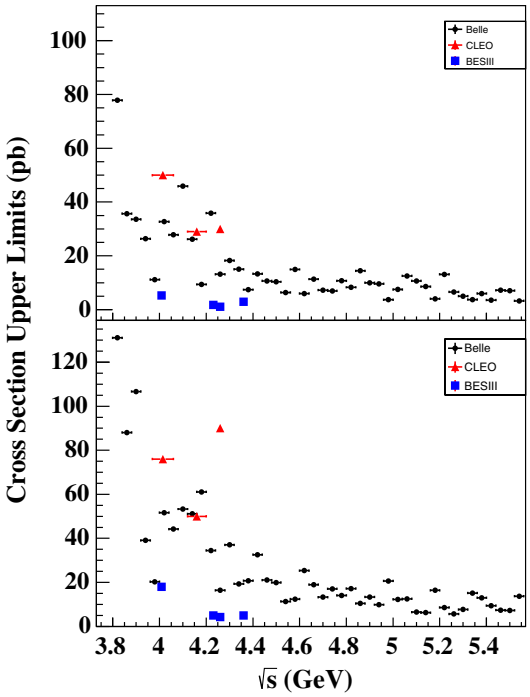


FIG. 7 (color online). Measured upper limits on the $e^+e^- \to \gamma\chi_{cJ}$ cross sections at the 90% C.L. for χ_{c1} (top) and χ_{c2} (bottom). The solid dots show the Belle measurements, the solid triangles are the results from CLEO, and the blue squares are from BESIII.

are two solutions for the best fit in this mode, and there are also two solutions in the $Y(4360)$ and $Y(4660)$ cases below], $\Gamma_{ee}[Y(4360)] \times \mathcal{B}[Y(4360) \to \pi^+\pi^-\psi(2S)] = (10.4 \pm 1.7 \pm 1.4)$ eV or $(11.8 \pm 1.8 \pm 1.4)$ eV [3], and $\Gamma_{ee}[Y(4660)] \times \mathcal{B}[Y(4660) \to \pi^+\pi^-\psi(2S)] = (3.0 \pm 0.9 \pm 0.3)$ eV or $(7.6 \pm 1.8 \pm 0.8)$ eV [3], we set the upper limits on the ratios of the branching fractions as shown in Table IV. The mass and width of the vector charmonium and charmoniumlike states, the background shape, and the fit range are varied in the fit to estimate the systematic uncertainties. The largest upper limit from these tests is taken as the final result. The total uncertainties from the reference processes and the systematic errors are considered by assuming they are Gaussian errors.

The following sources of systematic uncertainties are considered in the $\sigma(e^+e^- \to \gamma\chi_{cJ})$ upper-limit determination. The uncertainty in the tracking efficiency for tracks with angles and momenta characteristic of signal events is about 0.35% per track [11] and is additive. The uncertainty due to particle identification efficiency is 1.9%. The uncertainties of J/ψ mass and χ_{cJ} mass requirements are estimated using the $\psi(2S)$ sample in the same analysis and are found to be 1% and 1.3%, respectively. The generator EVTGEN is used in generating signal MC events. In this generator, however, only one ISR photon is allowed and the higher-order ISR effect should be estimated and corrected. This effect is studied by using a control sample $e^+e^- \to \gamma_{\rm ISR}\psi(2S)$ with $\psi(2S)$ decaying into $\eta J/\psi$. This process can be generated with both EVTGEN and PHOKHARA, a generator with higher-order ISR corrections. We assume that the correction factor obtained in this mode is the same as in the mode under study, and 9.0% is taken as the systematic error, corresponding to the uncertainty in the difference between the measured $\mathcal{B}(\psi(2S) \to \gamma\chi_{cJ} \to \gamma\gamma J/\psi)$ and the world average [17]. Taking the statistical error of the MC samples and the possible uncertainty in simulating the angular distributions of the full decay chain $\gamma\chi_{cJ} \to \gamma\gamma J/\psi$ into account, we quote a total uncertainty due to the generator as 12%. Belle measures luminosity with 1.4% precision and the trigger efficiency is about 91% with an uncertainty of 2%. Errors on the branching fractions of the intermediate states are taken from Ref. [17] with a systematic error of 4.5%. Assuming that these systematic error sources are independent, the total systematic error is 13.4%. The systematic uncertainty is considered in the upper limits shown in Tables I–IV.

TABLE I. Upper limits on the $e^+e^- \to \gamma\chi_{cJ}$ cross sections.

$\sqrt{s}$ (GeV)	χ_{c1} (pb)	χ_{c2} (pb)	$\sqrt{s}$ (GeV)	χ_{c1} (pb)	χ_{c2} (pb)
3.80–3.84	80	134	4.68–4.72	8	14
3.84–3.88	37	90	4.72–4.76	8	18
3.88–3.92	35	110	4.76–4.80	11	15
3.92–3.96	27	40	4.80–4.84	9	18
3.96–4.00	12	21	4.84–4.88	15	11
4.00–4.04	34	53	4.88–4.92	11	14
4.04–4.08	29	45	4.92–4.96	10	10
4.08–4.12	46	54	4.96–5.00	4	21
4.12–4.16	27	53	5.00–5.04	8	13
4.16–4.20	10	63	5.04–5.08	13	13
4.20–4.24	36	35	5.08–5.12	11	7
4.24–4.28	14	17	5.12–5.16	9	7
4.28–4.32	19	38	5.16–5.20	5	17
4.32–4.36	16	20	5.20–5.24	14	9
4.36–4.40	8	22	5.24–5.28	7	6
4.40–4.44	14	34	5.28–5.32	6	8
4.44–4.48	11	22	5.32–5.36	4	16
4.48–4.52	11	21	5.36–5.40	6	14
4.52–4.56	7	12	5.40–5.44	4	10
4.56–4.60	16	13	5.44–5.48	8	8
4.60–4.64	6	26	5.48–5.52	8	8
4.64–4.68	12	20	5.52–5.56	4	14

TABLE II. Upper limits on $\Gamma_{ee} \times \mathcal{B}$ at the 90% C.L.

	χ_{c1} (eV)	χ_{c2} (eV)
$\Gamma_{ee}[\psi(4040)] \times \mathcal{B}[\psi(4040) \to \gamma\chi_{cJ}]$	2.9	4.6
$\Gamma_{ee}[\psi(4160)] \times \mathcal{B}[\psi(4160) \to \gamma\chi_{cJ}]$	2.2	6.1
$\Gamma_{ee}[\psi(4415)] \times \mathcal{B}[\psi(4415) \to \gamma\chi_{cJ}]$	0.47	2.3
$\Gamma_{ee}[Y(4260)] \times \mathcal{B}[Y(4260) \to \gamma\chi_{cJ}]$	1.4	4.0
$\Gamma_{ee}[Y(4360)] \times \mathcal{B}[Y(4360) \to \gamma\chi_{cJ}]$	0.57	1.9
$\Gamma_{ee}[Y(4660)] \times \mathcal{B}[Y(4660) \to \gamma\chi_{cJ}]$	0.45	2.1

TABLE III. Upper limits on branching fractions $\mathcal{B}(R \to \gamma\chi_{cJ})$ at the 90% C.L.

Resonance	$\gamma\chi_{c1}$ (10^{-3})	$\gamma\chi_{c2}$ (10^{-3})
$\psi(4040)$	3.4	5.5
$\psi(4160)$	6.1	16.2
$\psi(4415)$	0.83	3.9

TABLE IV. Upper limits on branching fraction ratios at the 90% C.L. The two upper limits correspond to the two solutions in the reference processes.

Resonance	$\gamma\chi_{c1}$	$\gamma\chi_{c2}$
$\frac{\mathcal{B}[Y(4260)\to\gamma\chi_{cJ}]}{\mathcal{B}[Y(4260)\to\pi^+\pi^- J/\psi]}$	0.3 or 0.07	0.7 or 0.2
$\frac{\mathcal{B}[Y(4360)\to\gamma\chi_{cJ}]}{\mathcal{B}[Y(4360)\to\pi^+\pi^-\psi(2S)]}$	0.06 or 0.05	0.2 or 0.2
$\frac{\mathcal{B}[Y(4660)\to\gamma\chi_{c1}]}{\mathcal{B}[Y(4660)\to\pi^+\pi^-\psi(2S)]}$	0.2 or 0.07	0.9 or 0.3

In summary, using the full Belle data sample, we measure the $e^+e^- \to \gamma\chi_{cJ}$ process via initial state radiation. For the CM energy between 3.80 and 5.56 GeV, there are no significant $e^+e^- \to \gamma\chi_{c1}$ and $\gamma\chi_{c2}$ signals. The upper limits on the $e^+e^- \to \gamma\chi_{cJ}$ production cross sections, which range from a few pb to a few tens of pb, are set for the first time and are listed in Table I. We also set upper limits on the decay rate of the vector charmonium and charmoniumlike states to $\gamma\chi_{cJ}$. This information may help in understanding the nature of these vector states.

We thank the KEKB group for the excellent operation of the accelerator; the KEK cryogenics group for the efficient operation of the solenoid; and the KEK computer group, the National Institute of Informatics, and the PNNL/EMSL computing group for valuable computing and SINET4 network support. We acknowledge support from the Ministry of Education, Culture, Sports, Science, and Technology (MEXT) of Japan, the Japan Society for the Promotion of Science (JSPS), and the Tau-Lepton Physics Research Center of Nagoya University; the Australian Research Council and the Australian Department of Industry, Innovation, Science and Research; Austrian Science Fund under Grants No. P 22742-N16 and No. P 26794-N20; the National Natural Science Foundation of China under Grants No. 10575109, No. 10775142, No. 10875115, No. 11175187, and No. 11475187; the Chinese Academy of Science Center for Excellence in Particle Physics; the Ministry of Education, Youth, and Sports of the Czech Republic under Grant No. LG14034; the Carl Zeiss Foundation, the Deutsche Forschungsgemeinschaft and the VolkswagenStiftung; the Department of Science and Technology of India; the Istituto Nazionale di Fisica Nucleare of Italy; National Research Foundation (NRF) of Korea Grants No. 2011-0029457, No. 2012-0008143, No. 2012R1A1A2008330, No. 2013R1A1A3007772, No. 2014R1A2A2A01005286, No. 2014R1A2A2A01002734, and No. 2014R1A1A2006456; the Basic Research Lab program under NRF Grants No. KRF-2011-0020333 and No. KRF-2011-0021196, Center for Korean J-PARC Users, Grant No. NRF-2013K1A3A7A06056592; the Brain Korea 21-Plus program and the Global Science Experimental Data Hub Center of the Korea Institute of Science and Technology Information; the Polish Ministry of Science and Higher Education and the National Science Center; the Ministry of Education and Science of the Russian Federation and the Russian Foundation for Basic Research; the Slovenian Research Agency; the Basque Foundation for Science (IKERBASQUE) and the Euskal Herriko Unibertsitatea (UPV/EHU) under Grant No. UFI 11/55 (Spain); the Swiss National Science Foundation; the National Science Council and the Ministry of Education of Taiwan; and the U.S. Department of Energy and the National Science Foundation. This work is supported by a Grant-in-Aid from MEXT for Science Research in a Priority Area ("New Development of Flavor Physics") and from JSPS for Creative Scientific Research ("Evolution of Tau-lepton Physics").

[1] C. Z. Yuan *et al.* (Belle Collaboration), Phys. Rev. Lett. **99**, 182004 (2007).
[2] B. Aubert *et al.* (*BABAR* Collaboration), Phys. Rev. Lett. **95**, 142001 (2005); J. P. Lees *et al.* (*BABAR* Collaboration), Phys. Rev. D **86**, 051102 (2012).
[3] X. L. Wang *et al.* (Belle Collaboration), Phys. Rev. Lett. **99**, 142002 (2007).
[4] J. P. Lees *et al.* (*BABAR* Collaboration), Phys. Rev. D **89**, 111103 (2014).
[5] S. Godfrey and N. Isgur, Phys. Rev. D **32**, 189 (1985); T. Barnes, S. Godfrey, and E. S. Swanson, Phys. Rev. D **72**, 054026 (2005); G. J. Ding, J. J. Zhu, and M. L. Yan, Phys. Rev. D **77**, 014033 (2008).
[6] For a review, see N. Brambilla *et al.*, Eur. Phys. J. C **71**, 1534 (2011).
[7] T. E. Coan *et al.* (CLEO Collaboration), Phys. Rev. Lett. **96**, 162003 (2006).
[8] M. Ablikim *et al.* (BESIII Collaboration), Chin. Phys. C **39**, 041001 (2015).
[9] A. Abashian *et al.* (Belle Collaboration), Nucl. Instrum. Methods Phys. Res., Sect. A **479**, 117 (2002);

also see detector section in J. Brodzicka *et al.*, Prog. Theor. Phys. (**2012**) 04D001.

[10] S. Kurokawa and E. Kikutani, Nucl. Instrum. Methods Phys. Res., Sect. A **499**, 1 (2003), and other papers included in this Volume; T. Abe *et al.*, Prog. Theor. Phys. (**2013**) 03A001 and following articles up to 03A011.

[11] X. L. Wang *et al.* (Belle Collaboration), Phys. Rev. D **87**, 051101 (2013).

[12] D. J. Lange, Nucl. Instrum. Methods Phys. Res., Sect. A **462**, 152 (2001).

[13] G. Rodrigo, H. Czyż J. H. Kühn, and M. Szopa, Eur. Phys. J. C **24**, 71 (2002); S. Actis *et al.*, Eur. Phys. J. C **66**, 585 (2010).

[14] R. Brun *et al.*, GEANT3.21, CERN Report No. DD/EE/84-1, 1984.

[15] E. Nakano, Nucl. Instrum. Methods Phys. Res., Sect. A **494**, 402 (2002).

[16] A. Abashian *et al.*, Nucl. Instrum. Methods Phys. Res., Sect. A **491**, 69 (2002).

[17] K. A. Olive *et al.* (Particle Data Group), Chin. Phys. C **38**, 090001 (2014).

[18] E. A. Kuraev and V. S. Fadin, Yad. Fiz. **41**, 733 (1985) [Sov. J. Nucl. Phys. **41**, 466 (1985)].

[19] Z. Q. Liu *et al.* (Belle Collaboration), Phys. Rev. Lett. **110**, 252002 (2013).

[20] M. Ablikim *et al.* (BES Collaboration), Phys. Lett. B **660**, 315 (2008).